

# Quantitative structure-property relationship study of 1D-aligned soft magnetic nanocomposites for fast actuation

Yagmur Atescan<sup>1</sup>, Ricardo Braga Nogueira Branco<sup>1</sup>, Kohei Oyama<sup>1</sup>, Anna Madra<sup>2</sup>, and Namiko Yamamoto<sup>3</sup>

The Pennsylvania State University, University Park, PA, 16802, USA

Soft magnetic composites, consisting of magnetic particles in elastomer matrices, are of interests as an alternative actuator to aerospace engineering applications, due to their flexibility, fast actuation, and light weight. Their magnetostriction performance is largely affected by particle organization within the composites, and methods to eliminate demagnetization to maximize such actuation performance is currently not well understood. In this work, relationships between the particle organization and the magnetic susceptibility are experimentally studied about soft magnetic composites with aligned maghemite nanoparticles, in a quantitative manner. The preliminary results indicate compatibility with the hypothesis where inner demagnetization can be decreased by particle alignment with less agglomeration.

#### I. Nomenclature

 $C_k$  [unitless] = volume fraction of the kth element within a composite

H [Oe] = applied magnetic field Hc [emu] = coercivity of a composite

 $H_{k\alpha}$  [A/m] = magnetic field within the kth element of a composite along  $\alpha$  direction ( $\alpha = x, y, z$ )

Lx [m] = length of a composite along the particle alignment direction

Ly [m] = width of a composite Lz [m] = height of a composite  $m_c$  [kg] = mass of a composite  $m_p$  [kg] = mass of particles

M [emu] = measured magnetization of a composite  $M_{sat}$  [emu] = saturation magnetization of a composite

 $N_{k\alpha}$  [unitless] = shape factor of the kth element within a composite along  $\alpha$  direction ( $\alpha = x, y, z$ )

 $N_{m\alpha}$ [unitless] = shape factor of a polymer matrix within a composite along  $\alpha$  direction.

 $N_{p\alpha}$  [unitless] = shape factor of a particle within a composite along  $\alpha$  direction.

 $\begin{array}{lcl} \textit{V}_{c} \ [m^{3}] & = & \text{volume of a composite} \\ \textit{V}_{p} \ [m^{3}] & = & \text{volume of particles} \\ \textit{\rho}_{c} \ [\text{kg/m}^{3}] & = & \text{density of a composite} \\ \textit{\rho}_{m} \ [\text{kg/m}^{3}] & = & \text{density of a matrix} \\ \textit{\rho}_{p} \ [\text{kg/m}^{3}] & = & \text{density of particles} \end{array}$ 

 $\phi$  [vol%] = volume fraction of particles in a composite  $\chi_{mass}$  [m³/kg]= initial mass susceptibility of a composite  $\chi_{v}$  [unitless] = initial volume susceptibility of a composite

<sup>&</sup>lt;sup>1</sup> Graduate Research Assistant, Department of Aerospace Engineering, and Student Member.

<sup>&</sup>lt;sup>2</sup> Postdoctoral Researcher, Department of Civil Engineering.

<sup>&</sup>lt;sup>3</sup> Associate Professor, Department of Aerospace Engineering, and Senior Member.

 $\chi_p[\text{unitless}] = \text{magnetic susceptibility of a particle}$   $\chi_m[\text{unitless}] = \text{magnetic susceptibility of a polymer matrix}$   $\chi_{e\alpha}[\text{unitless}] = \text{effective magnetic susceptibility of a composite along } \alpha \text{ direction}$   $\chi_k[\text{unitless}] = \text{magnetic susceptibility of the } k\text{th element within a composite}$   $\mu_0[\text{N/A}^2] = \text{magnetic permeability of free space}, \mu_0 = 4\pi \times 10^{-7} [\text{N/A}^2]$   $\mu_{e\alpha}[\text{N/A}^2] = \text{effective magnetic permeability of a composite along } \alpha \text{ direction}$   $\mu_k[\text{N/A}^2] = \text{magnetic permeability of the } k\text{th element within a composite}$ 

# II. Introduction

A erospace applications require actuators capable of large displacements, precise positioning and fast response times, high specific energy density, low power consumption, active damping of vibration, and more [1]. Shape memory alloys (SMAs) and piezoelectric materials are commonly used as such actuator materials. As summarized in Figure 1 [2, 3], SMAs have high specific energy density, but its response time is slow, and large temperature change is required for actuation. On the other hand, piezoelectric actuators respond faster, but specific energy density is lower [4]. In addition, the electrical poling procedure to enable piezoelectric responses can be complicated due to the high dielectric constant of most ferroelectric fillers [5]. Here, soft magnetic composites (SMCs) are a new class of actuator that can provide faster actuation response than SMA and larger specific energy density than piezoelectric polymer (PVDF) [6, 7].

SMCs consist of particles with soft magnetism (such as soft magnetic ferrites or metals) embedded in a non-magnetic polymer matrix. Their magnetostriction performances are determined by the magnetic properties of the particles, and are also largely by particle distribution (volume fraction, organization, agglomeration, etc.) within the matrix. For example, the magnetic susceptibility of a SMC with aligned particles is higher than that of a SME with randomly oriented particles, achieving higher magnetostriction [8]. However, correlation between these particle structures and the magnetic susceptibility and magnetostriction behaviors are not fully understood yet, especially when the particle volume fraction is small. The measured susceptibility and magnetostriction are smaller than those calculated based on magnetic contribution of the particles, due to demagnetization from local particle interactions [9, 10].

In this work, the relationships between the particle organization with the susceptibility of SMCs are experimentally studied, as the first step to understand methods to minimize demagnetization and maximize actuation. The general demagnetization of the composite, inner demagnetization can be decreased by providing percolation along the actuation direction of interests. SMCs with more precisely tailored particle structures were fabricated by improved particle dispersion with surface treatment and by application of uniaxial and homogeneous magnetic fields with a Helmholtz coil system. The particle structures in SMCs were inspected using microCT scan, and these scanned images and the particle structures were quantitatively characterized. Anisotropic susceptibility data, an indication of magnetostriction, of SMCs were measured using vibrating sample magnetometry (VSM), and compared with the particle structures.

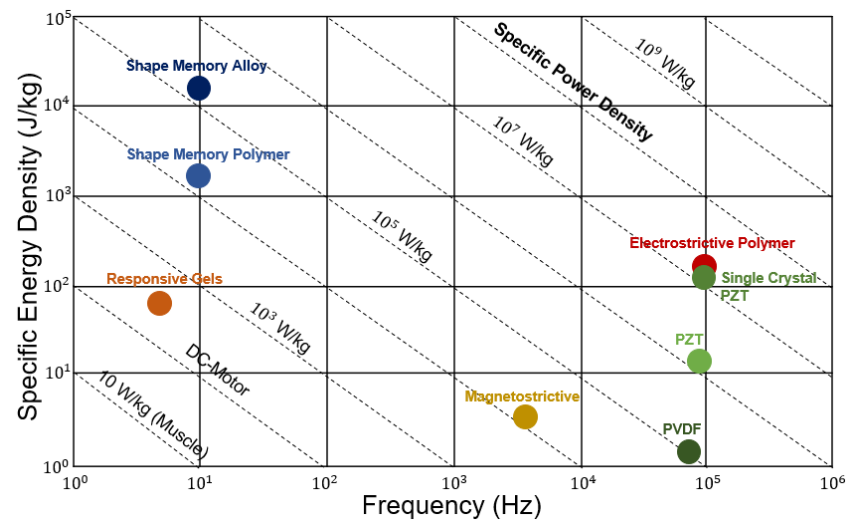
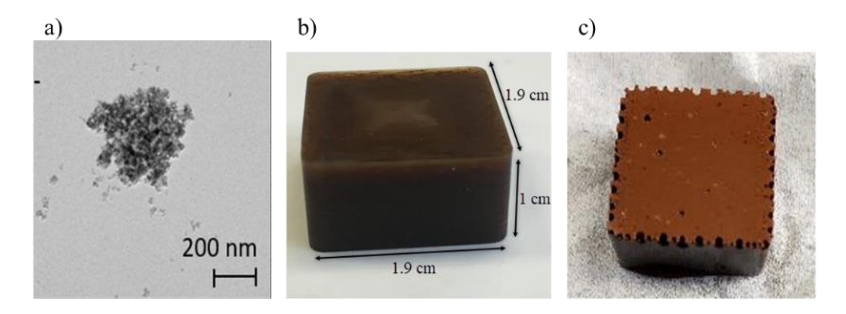


Fig. 1 Comparison of actuator performance, created based on [11].

## III. Fabrication of SMCs with aligned maghemite nanoparticles

Model polymer nanocomposites were prepared with maghemite nanoparticles (US Research Nanomaterials, US3200, γ-Fe<sub>2</sub>O<sub>3</sub>, ~25 nm diameter), because this ferromagnetic nanoparticle can be easily assembled using externally applied magnetic fields in viscous polymer matrices. Two different polymers were used as the matrix, separately (see Figure 2): PDMS (polydimethylsiloxane, Elastosil RT 604A and 694B, Wacker, soft, aimed for actuation applications), and epoxy (bisphenol-F type, EPON 862, Miller-Stephenson, rigid, suitable for aerospace structure applications). To note, the epoxy is not soft, and was used only as a model matrix to study the structure-property relationship in this work. The detailed fabrication processes can be found elsewhere [12, 13]. The as-received nanoparticles forms aggregate with the size of ~100s of nm, due to magnetic remanence (see Figure 2a). To mitigate agglomeration in these matrices, the maghemite nanoparticles were surface-modified using silane coupling agents: 3-(Trimethoxysilyl)propyl methacrylate (TMM, Dow Corning) for the PDMS, and 3-glycidyloxypropyl trimethoxysilane (GPS, Sigma-Aldrich) for the epoxy. The surface-modified maghemite nanoparticles (4900 kg/m<sup>3</sup>) were intensively mixed with each polymer matrix (PDMS of 970 kg/m<sup>3</sup>, and epoxy of 1167 kg/m<sup>3</sup>) using ultrasonication (Branson 1800, 50 °C, 40 kHz) and centrifugal mixer (Thinky Planetary Centrifugal Mixer ARE-310, Immediately after mixing and before curing, these maghemite-polymer mixtures were poured into an aluminum mold (1.91 cm × 1.91 cm × 0.95 cm), and placed inside a Helmholtz coil system (MicroMagnetics) to apply a uniaxial magnetic field at elevated temperatures to decrease the polymer viscosity; the field conditions are summarized in Table 1. After magnetic assembly, the mixture was cured and post-cured following the cycles provided by the polymer manufacturers.



**Fig. 2** Fabrication of maghemite SMCs: a) transmission microscope image of maghemite nanoparticles and agglomerate, and digital images of b) a maghemite-PDMS SMC and c) a maghemite-epoxy SMC.

**Table 1.** Fabrication conditions of maghemite SMC.

Sample	Field applied in the x direction for assembly	Field direction applied for measurement	Nanoparticle volume fraction \$\phi [vol%]	Initial volume susceptibility of SMC $\chi_v$
<b>Reference PDMS</b>				
Randomly oriented	None	X	0.47	3.46E-02
		у	0.47	3.85E-02
		Z	0.45	3.30E-02
		X	0.41	2.98E-02
PDMS SMC				
1D aligned in the x direction	Static 300 G	X	0.51	7.65E-02
	40 °C for 15 min	у	0.47	2.85E-02
	70 °C for 30 min	Z	0.46	2.67E-02
	Oscillating (0.05 Hz) 300 G	X	0.52	7.76E-02
	40 °C for 15 min	y	0.48	2.70E-02
	70° C for 30 min	Z	0.45	2.65E-02
Without	Static 300 G	X	0.10	8.30E-03
functionalization,	40 °C for 15 min	y	0.12	5.43E-03
1D aligned	70 °C for 30 min	Z	0.12	5.62E-03

in the x direction		X	1.00	1.10E-01
		У	1.05	5.41E-02
Epoxy SMC				
1D aligned in the x direction	Static 300 G 70 °C for 30 min 121 °C for 60 min	X	0.24	2.99E-02
		У	0.24	1.91E-02
		Z	0.24	1.90E-02
		X	3.92	5.23E-01
		У	4.46	3.70E-01
		Z	4.77	3.91E-01
	Oscillating (0.05 Hz) 300 G 70 °C for 30 min 121 °C for 60 min	X	0.21	2.57E-02
		У	0.22	1.82E-02
		Z	0.20	1.70E-02
		X	4.15	5.03E-01
		У	4.33	3.64E-01
		Z	4.07	3.46E-01

# IV. Magnetic property measurement of maghemite SMCs

The prepared maghemite SMCs were tested using vibrating sample magnetometry (VSM, MicroSense), to measure the maghemite volume fraction and the initial magnetic susceptibility. From each SMC with maghemite nanoparticles aligned in one direction (x), three cubic pieces ( $\sim$ 3-4 mm  $\times$  3-4 mm) were prepared to measure their anisotropic magnetic properties; one cut piece was applied with the field only in one of the three directions (x, y and z) to measure the magnetic property only of that direction and to avoid remanence. The applied magnetic field was cycled from 0 Oe, 18 kOe, -18 kOe, and then back up to 18 kOe for the maghemite SMCs. The step size of the applied field was varied to capture the rapid magnetization change within the small field range and accurately measure the initial susceptibility:  $\sim$ 1 Oe step for |H| < 100 Oe,  $\sim$ 10 Oe step for 100 Oe < |H| < 1 kOe,  $\sim$ 250 Oe step for 1 kOe < |H| < 8 kOe, and  $\sim$ 1 kOe step for 8 kOe < |H| < 18 kOe. In addition to the 1D-aligned maghemite SMCs, two reference samples were also prepared: the randomly-oriented maghemite-PDMS SMC prepared without magnetic fields, and the maghemite nanoparticles by themselves without polymers. For the maghemite nanoparticles, the magnetic field was cycled from 0 kOe, 18 kOe, -18 kOe, and then back up to 18 kOe; the step sizes were set as  $\sim$ 1 Oe step for |H| < 0.1 kOe,  $\sim$ 10 Oe step for 0.1 kOe < |H| < 1 kOe,  $\sim$ 250 Oe step for 1 kOe < |H| < 8 kOe and  $\sim$ 1 kOe step for 8 kOe < |H| < 1 kOe,  $\sim$ 10 Oe step for 0.1 kOe < |H| < 1 kOe,  $\sim$ 250 Oe step for 1 kOe < |H| < 1 kOe step for 8 kOe < |H| < 1 kOe.

First, the magnetic properties of the maghemite nanoparticles were characterized from the H-M plots (see **Figure 3a**). The saturation magnetization was measured by extrapolating the measurement in the high H range of 10-18 kOe using the simplified version of law of approach to saturation [14], knowing maghemite is ferromagnetic:  $M = M_{sat}(1-p/H)$  where p is a constant. As plotted in **Figure 3b**, the  $M_{sat}$  of the reference maghemite nanoparticles ( $m_p = 0.116$  [g] =  $1.16 \times 10^{-4}$  [kg]), without the polymer, was estimated as 7.77 [emu]. The initial mass susceptibility  $\chi_{mass}$  [m<sup>3</sup>/kg] of the maghemite nanoparticles is calculated from the slope of the H-M plot (see **Figure 3c**, M [emu] and H [Oe], where 1 [emu] =  $10^{-3}$  [ $A \cdot m^2$ ] and 1 [Oe] =  $\frac{1000}{4\pi}$  [A/m]) in the low, or initial, H range of 0 to 25 Oe, using the equation below.

$$\chi_{mass} [m^{3}/kg] = \frac{M[emu] \cdot 10^{-3} [A \cdot m^{2}/emu]}{H[Oe] \cdot \frac{1000}{4\pi} [A/m/Oe]} \cdot \frac{1}{m_{p}[kg]} = \frac{4\pi}{10^{6}} \left[ \frac{A \cdot \frac{m^{2}}{emu}}{\frac{A}{Oe}} \right] \cdot \frac{M[emu]}{H[Oe]} \cdot \frac{1}{m_{p}[kg]} \dots (1)$$

The initial volume susceptibility  $\chi_v$  [unitless] can then be calculated as following:

$$\chi_v = \chi_{mass} \left[ m^3 / kg \right] \cdot \rho_p \left[ \frac{kg}{m^3} \right] \dots (2)$$

The initial susceptibility values of maghemites were calculated as  $\chi_{mass} = 9.21 \times 10^{-4} [m^3/kg]$  and  $\chi_v = 4.51$ .

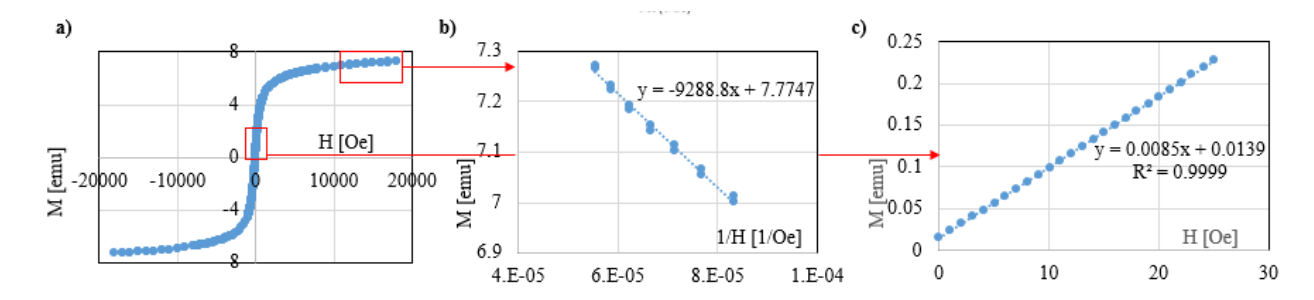


Fig. 3 VSM measurement of maghemite nanoparticles without polymers ( $m_p$  of  $1.16 \times 10^{-4}$  [kg]): a) H-M plot over  $\pm 18$  kOe, b) 1/H-M plot for  $M_{sat}$  calculation, and c) H-M plot over 0-25 Oe for initial susceptibility measurement.

Second, the H-M plots of the maghemite SMCs were processed. Considering that the polymer matrix is not magnetic, the magnetization value should be attributed only the maghemite particles. The  $M_{sat}$  of the SMC was calculated in the same manner as the maghemite nanoparticles. The mass of the maghemite nanoparticles in the SMCs were calculated by comparing their saturated magnetization values ( $M_{sat}$ ) with that of the reference maghemite nanoparticles, using the following equation.

$$\begin{split} m_p & \text{ in composite } [kg] = \frac{(M_{sat} \text{ of } SMC \text{ } [emu])}{(M_{sat} \text{ of } maghemites \text{ } [emu])} \cdot \left(m_p \text{ of } maghemites \text{ } [kg]\right) \\ &= \frac{(M_{sat} \text{ of } SMC \text{ } [emu])}{7.77 \text{ } [emu]} \cdot \left(1.16 \cdot 10^{-4} \text{ } [kg]\right) \\ &= (M_{sat} \text{ of } SMC \text{ } [emu]) \cdot \left(1.49 \cdot 10^{-5} \left[\frac{kg}{emu}\right]\right) \dots (3) \end{split}$$

The volume fraction of the maghemite nanoparticles were calculated using the following equation:  $\rho_p$  is the density of the maghemite nanoparticles (4900 [kg/m<sup>3</sup>]),  $\rho_m$  is the density of the matrix, and  $m_c$  is the mass of the SMC [kg].

$$\phi = \frac{V_{p}[m^{3}]}{V_{c}[m^{3}]} = \frac{(m_{p} \, in \, SMC \, [kg])/\rho_{p}[\frac{kg}{m^{3}}]}{\frac{m_{p} \, in \, SMC \, [kg]}{\rho_{p}\left[\frac{kg}{m^{3}}\right]} + (m_{c} - \left(m_{p} \, in \, SMC \, [kg]\right))/\rho_{m}[\frac{kg}{m^{3}}]} \dots (4)$$

The initial susceptibilities of composites are calculated with the similar manner as the case of maghemite, but this time with the SMC mass  $m_c$  and the SMC density  $\rho_c$ . The measurement results are summarized in **Table 1**.

$$\chi_{mass}\left[m^3/kg\right] = \frac{4\pi}{10^6} \left[\frac{A \cdot m^2/emu}{A/m/0e}\right] \cdot \frac{M[emu]}{H[0e]} \cdot \frac{1}{m_c[kg]} \dots (5)$$

#### V. Quantitative characterization of heterogeneous 1D structures of maghemite particles

MicroCT scan was conducted on SMCs to inspect maghemite nanoparticle structures (GE Phoenix vtome XL, at the Center for Quantitative Imaging at Pennsylvania State University) [15]. For the PDMS SMCs, rectangular samples of 3 mm  $\times$  3 mm  $\times$  5 mm were cut out from the bottom edge of the as-fabricated SMCs. The measurement parameters were set as follows: focus-to-detector distance (FDD) as 550 mm, focus-to-object distance (FOD) as 8.25 mm, and the X-ray beam acceleration voltage as 80 keV. The voxel resolution of 3  $\mu$ m  $\times$  3  $\mu$ m  $\times$  3  $\mu$ m was obtained with a 66x magnification. For the epoxy SMCs, approximately quarter-sized samples (9.6 mm  $\times$  9.6 mm  $\times$  9.5 mm) were extracted from the original bulk composites. The measurement parameters were set as follows: FDD as 525 mm, FOD as 21 mm, and the X-ray beam acceleration voltage as 100 keV. The voxel resolution of approximately 8  $\mu$ m  $\times$  8  $\mu$ m  $\times$  8  $\mu$ m was obtained with a 25x magnification. The voxel resolutions of 3  $\mu$ m and 8  $\mu$ m are still low and cannot capture individual nanoparticle aggregates and small nanoparticle assembly line widths. The voxel resolution can be reduced by decreasing the sample volume size to the limit of detector sensitivity, but the current sample dimensions were kept in this work to capture the heterogeneous nanoparticle structures across the samples.

Quantitative information about these nanoparticle structures were obtained by processing the microCT data, by using Trainable Weka Segmentation available in ImageJ/Fiji software package and through automated voxel classification (nanoparticles, matrix, or pore) with machine learning algorithm Fast Random Forest [16, 17]. A clustering segmentation using machine learning was performed by first manually selecting representative phases (for example, nanoparticle vs. matrix). These representative phases information was used as training data for Fast Random Forest learning algorithm. Classification rules were then applied to the training data based upon the phase identified attenuation coefficients and a set of convolutions (Gaussian, Laplacian, and Sobel). An exemplary segmentation processed image is compared with the reference original microCT tomogram in **Figure 4**. Segmented microCT images were processed using in-house Matlab code in order to quantitatively evaluate the volume fraction of nanoparticles within the samples and assembly sizes (length, width, and separation) [18]. The volume fraction of nanoparticles calculated from the algorithm were, on average, approximately 3 times greater than those directly calculated from VSM test results. This discrepancy is attributed to a transition region found between the assemblies and the matrix which produces a slight shadowing in the microCT images and low resolution of microCT images.

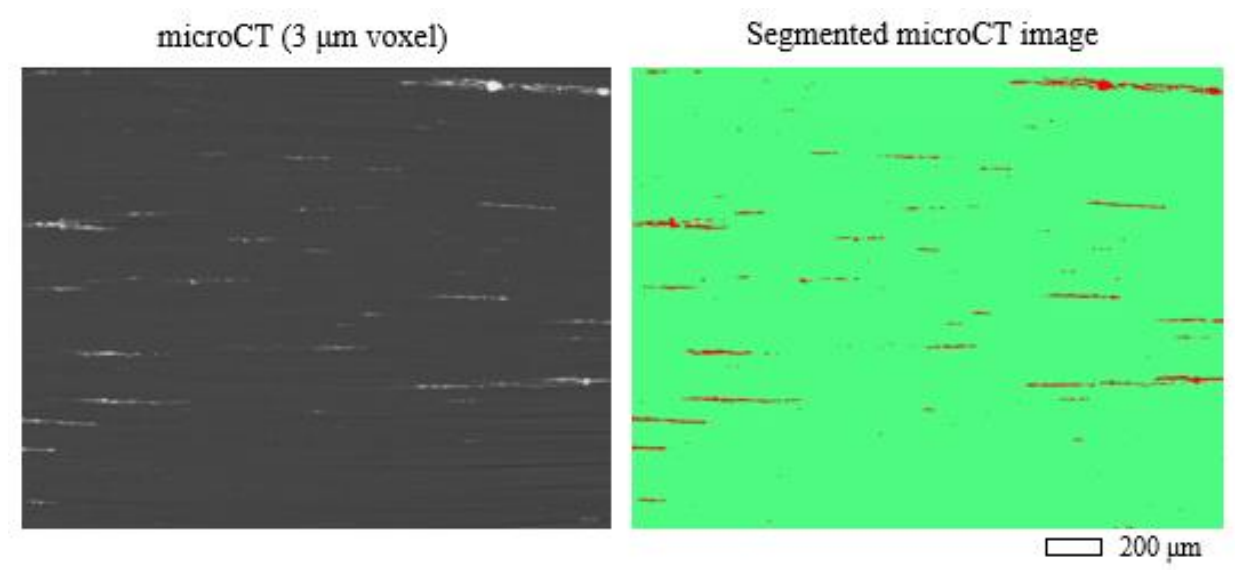


Fig. 4 Comparison of the reference microCT scan image, and the microCT scan image with segmentation process.

#### VI. Theoretical evaluation of SMCs magnetization effectiveness

Magnetic effectiveness of particle-matrix composites is determined by how magnetic particles are distributed within the composite, as well as the composite sample shape. Magnetization gap emerges when an individual magnetic particle is submerged inside a non-magnetic matrix, causing demagnetization. Thus, particle distributions, orientations, and volume fractions collectively determine this *inner* demagnetization effect of the composite. Meanwhile, the magnetic poles on the composite sample surface also cause demagnetization. This *outer* demagnetization effect is determined by the composite sample shape, as well as particle distribution and volume fraction (percolation threshold). The combined effect of inner and outer demagnetization decreases effectiveness of magnetization by particle introduction, and such effect can be observed with experimentally obtained magnetic susceptibility data of the composites [10, 19]. In this study, magnetic poles on the composite surface are low due to low volume fraction of maghemite particles. Thus, contribution of outer demagnetization is assumed as small. Only inner demagnetization effect due to particle distribution and orientation was taken into consideration in this work. In SMCs, multiple particles of different shapes and orientations are distributed within a "composite" matrix. The effective property and magnetization of the composite in the  $\alpha$  direction (where  $\alpha$  can be either  $\alpha$ ,  $\alpha$ , or  $\alpha$ ) can be calculated by adding the magnetization contribution of all the particles and the matrix using the self-consistent law as described in **Equation 6** (effective medium theory) [19].

$$\sum_{k=1,2,\dots} C_k \mu_k H_{k\alpha} = \sum_{k=1,2,\dots} C_k \mu_{e\alpha} H_{e\alpha} \cdots (6)$$

Here,  $C_k$  stands for the volume fraction of the kth element and of the matrix if the matrix is magnetically responsive. Magnetic field  $H_{k\alpha}$  within a kth element (particle or matrix) within a composite in the  $\alpha$  direction can be described as in **Equation 7**.

$$H_{k\alpha} = \frac{\mu_{e\alpha}}{\mu_{e\alpha} + N_{k\alpha}(\mu_k - \mu_{e\alpha})} H_{e\alpha} \cdots (7)$$

 $\mu_k$  is the permeability of the kth element, and  $\mu_{e\alpha}$  is that of the effective composite in the  $\alpha$  direction.  $H_{e\alpha}$  is the effective magnetic field within the composite in the  $\alpha$  direction. The effective permeability  $\mu_{e\alpha}$  and the magnetic field  $H_{e\alpha}$  of a composite can be different about each direction (x, y, or z) due to anisotropic particle distribution. The shape factor of the kth element in the  $\alpha$  direction is described as  $N_{k\alpha}$ ; even when the shape is the same for all the particles, their orientation can be varied.  $N_{k\alpha}$  can be described as in **Equations 8** and **9** for prolate spheroid (shape of prolate spheroid is compatible enough with 1D aligned particle aggregates). The parallel (to the long axis) and perpendicular shape factors for a prolate spheroid (x>y=z), having an aspect ratio m=x/y, are calculated using the following equations.

$$\begin{split} N_{x,prolate} &= \frac{1}{m^2 - 1} \left[ \frac{m}{\sqrt{m^2 - 1}} In\left(m + \sqrt{m^2 - 1}\right) - 1 \right] \dots (8) \\ N_{y,prolate} &= N_{z,prolate} = \frac{1 - N_x}{2} \dots (9) \end{split}$$

Combining **Equations 6** and **7**, the following **Equation 10** was extracted.  $\chi_{e\alpha}$  is the susceptibility of the composite in the  $\alpha$  direction, and  $\chi_k$  is that of the kth element within the composite. The effective composite susceptibility can be estimated based on the particle volume fraction, shape, and orientation using **Equation 10** of EMT.

$$\sum_{k=1,2,...} C_k \left( \mu_k \frac{\mu_{e\alpha}}{\mu_{e\alpha} + N_{k\alpha}(\mu_k - \mu_{e\alpha})} - \mu_{e\alpha} \right) H_{e\alpha} = \sum_{k=1,2,...} C_k \left( \frac{(1 - N_{k\alpha})(\chi_k - \chi_{e\alpha})}{1 + \chi_{e\alpha} + N_{k\alpha}(\chi_k - \chi_{e\alpha})} \right) = 0 \cdots (10)$$

In this study, maghemite particles with particle susceptibility,  $\chi_p = 4.51$  and polymer matrix with  $\chi_m = 0$  (non-magnetic) were used. Due to the bulk cubic shape of matrix (VSM test samples were 3-4 mm x 3-4 mm x 3-4mm), shape factor of matrix was assumed to be constant at each direction and equal to shape factor of a sphere,  $N_{m\alpha} = 0.33$ . Shape factor of particle assemblies,  $N_{p\alpha}$  were calculated using length and width information that were obtained from evaluation of microCT images which was stated in section V. Length and width of each particle assemblies were used to calculate aspect ratio (m). Shape factor of particle assemblies  $N_{p\alpha}$ , were calculated for each particle assembly using **Equation 8**. Susceptibility of the composite,  $\chi_{e\alpha}$  was then solved using **Equation 9**. From the large data of microCT images, 3 random image sets (each with 20 images) were selected to evaluate the length and width of particle aggregates, and then used those values to calculate the susceptibility of the composite. Validity of these image sampling was checked using the probability density; the probability density of particle assembly aspect ratio sizes was comparable for the selected image sets and the whole microCT image stack (see **Figure 5**).

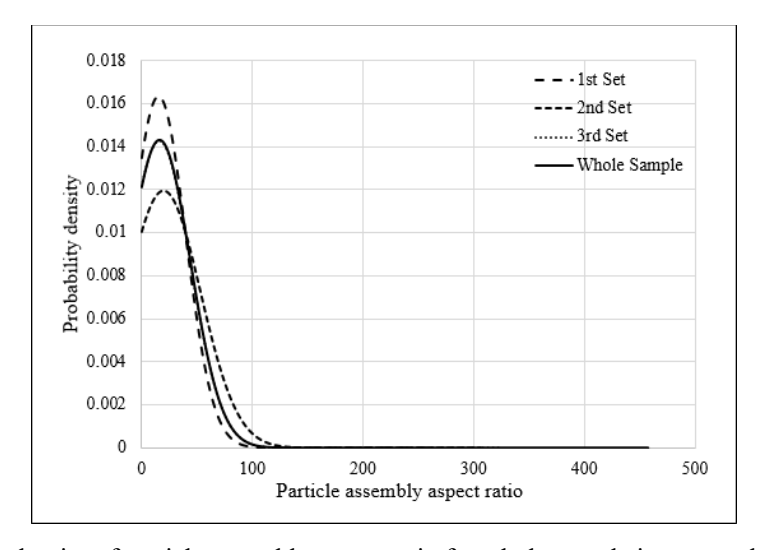


Fig. 5 Probability density of particle assembly aspect ratio for whole sample image stack and 3 image sets.

## VII. Analysis of measured and theoretically calculated magnetic properties of maghemite SMCs

The above results are currently studied in comparison with previous measurement data, with theoretical estimation, and also with the measured nanoparticle structures observed from the microCT scan images. As for the theoretical model, effective medium theory to consider inner demagnetization effects of SMCs is studied [18]. As compared in Figure 6, magnetic susceptibility values of the 1D-aligned maghemite-PDMS SMCs exhibit higher values in the particle alignment direction than those of the randomly-oriented maghemite-PDMS SMC, but also exhibit lower values in the direction perpendicular to the particle alignment. This trend is more emphasized with functionalization of particles and thus with smaller aggregate size. Quantified evaluation of hierarchical nanoparticle structures from microCT images is performed to evaluate theoretical results for composite susceptibility. As compared in Table 2, theoretical magnetic susceptibility values of the 1D-aligned functionalized maghemite-PDMS SMC shows similar results for all image sets. Even though both experimental and theoretical values are in the same scale, theoretical results exhibit smaller values than the experimental values. This discrepancy is attributed to errors in microCT image analysis process and assumptions on theoretical calculations.

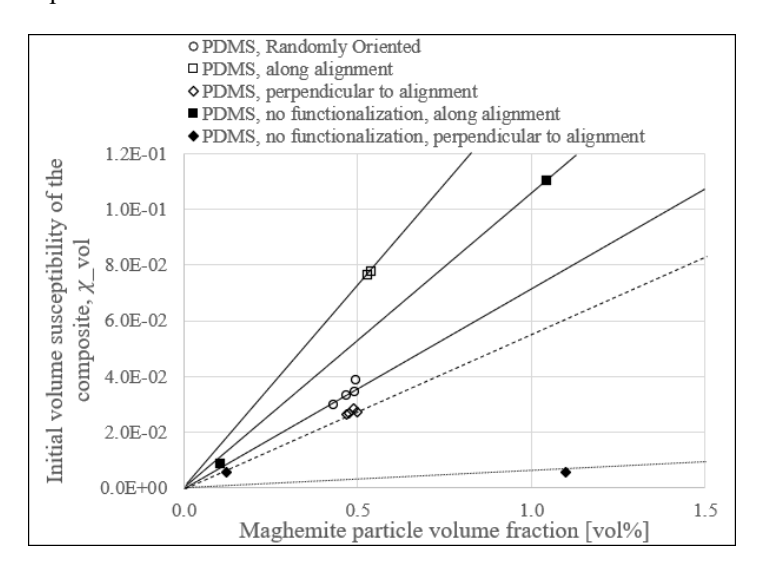


Fig. 6 Comparison of the measured initial susceptibility values of maghemite-PDMS SMCs.

**Table 2.** Comparison of experimental and theoretical volume susceptibility results.

Sample	Experimental	1st Set	2 <sup>nd</sup> Set	3 <sup>rd</sup> Set
1D PDMS – Along alignment	0.0784	0.0236	0.0243	0.0231
1D PDMS – Perpendicular to alignment	0.0287	0.0073	0.0071	0.0074

#### VIII. Conclusion

The goal of this study is to better understand the magnetization effectiveness of SMCs with aligned maghemite nanoparticles and provide methods to eliminate demagnetization to maximize actuation performance. For this purpose, relationships between the particle organization and the magnetic susceptibility were experimentally studied about SMCs with aligned maghemite nanoparticles, in a quantitative manner. A uniform dispersion was obtained by surface treatment of maghemite nanoparticles with silane coupling agents. Magnetic organization of a low volume fraction maghemite nanoparticles within high viscosity polymers was achieved. MicroCT scans of SMC samples were provided to better understand the particle organization within the composites. Quantitative information about these assemblies were obtained by processing the microCT data, by using Trainable Weka Segmentation available in ImageJ/Fiji software package and through automated voxel classification (nanoparticles, matrix, or pore) with machine learning algorithm Fast Random Forest. Effects of anisotropic particle structures on magnetic susceptibility of SMCs were investigated using Vibrating Sample Magnetometer (VSM). The evaluated nanoparticle structure and

magnetic properties of SMCs were compared with analytical studies. The preliminary results indicate compatibility with the hypothesis where inner demagnetization can be decreased by particle alignment with less agglomeration.

Future work will include additional studies on triaxial magnetic field assembly of particles. Anisotropic actuation properties of the fabricated SMCs will be defined with magnetostriction measurements. Further quantitative characterization of microCT images will be performed to mitigate demagnetization and thus maximize magnetostriction actuation.

## Acknowledgments

This material is based upon work supported by the National Science Foundation under Grant No. 1844670, and by College of Engineering, the Penn State University. Yagmur Atescan is thankful for the financial support of The Scientific and Technological Research Council of Turkey – BIDEB 2213 scholarship. The authors would also like to thank Prof. Paris von Lockette and Mr. Corey Breznak (Mechanical Engineering, Penn State) for their assistance with VSM measurement, and Mr. Tim Stecko (the Quantitative Imaging Laboratory, Penn State) for his assistance with the microCT measurements.

#### References

- 1. Bouchilloux, P., F. Claeyssen, and R. Le Letty. *Amplified piezoelectric actuators: From aerospace to underwater applications.* in *Smart Structures and Materials 2004 Conference.* 2004. San Diego, CA.
- 2. Hartl, D.J. and D.C. Lagoudas, *Aerospace applications of shape memory alloys*. Proceedings of the Institution of Mechanical Engineers Part G-Journal of Aerospace Engineering, 2007. **221**(G4): p. 535-552.
- 3. Kim, H.A., et al., Shape Memory Alloy-Piezoelectric Active Structures for Reversible Actuation of Bistable Composites. Aiaa Journal, 2010. **48**(6): p. 1265-1268.
- 4. Patel, I., E. Siores, and T. Shah, *Utilisation of smart polymers and ceramic based piezoelectric materials for scavenging wasted energy.* Sensors and Actuators a-Physical, 2010. **159**(2): p. 213-218.
- 5. Ribeiro, C., et al., *Piezoelectric poly(vinylidene fluoride) microstructure and poling state in active tissue engineering*. Engineering in Life Sciences, 2015. **15**(4): p. 351-356.
- 6. Bose, H., R. Rabindranath, and J. Ehrlich, *Soft magnetorheological elastomers as new actuators for valves.* Journal of Intelligent Material Systems and Structures, 2012. **23**(9): p. 989-994.
- 7. Erb, R.M., et al., *Actuating Soft Matter with Magnetic Torque*. Advanced Functional Materials, 2016. **26**(22): p. 3859-3880.
- 8. Yagmur Atescan, N.Y. 3D Structuring of Magnetoelastomers for Anisotropic Actuation Properties. in 61st AIAA/ASCE/AHS/ASC Structures, Structural Dynamics, and Materials Conference. 2020. San Diego, CA.
- 9. Lin, G.Q., et al., *Influence of demagnetizing field on the permeability of soft magnetic composites*. Journal of Magnetism and Magnetic Materials, 2006. **305**(2): p. 291-295.
- 10. M. Anhalt, B.W., J. L. Mattei, *Inner demagnetizing factor in polymer bonded soft magnetic composites*, in 18th Soft Magnetic Material Conference. 2007: United Kingdom.
- 11. Fan, Y., Multi-scale approaches for the vibration and energy flow through piezoelectric waveguides: simulation strategies, control mechanisms and circuits optimization, in Mechanics. 2016, Beihang University. p. 257.
- 12. Stepanov, G.V., et al., Effect of a homogeneous magnetic field on the viscoelastic behavior of magnetic elastomers. Polymer, 2007. **48**(2): p. 488-495.
- 13. Yang, J., et al., *Development and evaluation of an MRE-based absorber with two individually controllable natural frequencies.* Smart Materials and Structures, 2018. **27**(9).
- 14. Zhang, H., D.C. Zeng, and Z.W. Liu, *The law of approach to saturation in ferromagnets originating from the magnetocrystalline anisotropy*. Journal of Magnetism and Magnetic Materials, 2010. **322**(16): p. 2375-2380.
- 15. Gunther, D., et al., *X-ray micro-tomographic characterization of field-structured magnetorheological elastomers*. Smart Materials and Structures, 2012. **21**(1).
- 16. Madra, A., N. El Hajj, and M. Benzeggagh, *X-ray microtomography applications for quantitative and qualitative analysis of porosity in woven glass fiber reinforced thermoplastic*. Composites Science and Technology, 2014. **95**: p. 50-58.
- 17. Madra, A., Breitkopf, Maire, Trochu, *A clustering method for analysis of morphology of short natural fibers in composites based on X-ray microtomography*. Compos. Part A Appl. Sci. Manuf., 2017: p. 184-195.
- 18. Spencer, M.P., SCALABLE MANUFACTURING OF POLYMER NANOCOMPOSITES USING OSCILLATING MAGNETIC FIELDS, in Aerospace Engineering. 2019, The University of Pennsylvania.

19. Mattei J-L, L.F.h.M., *Effects of the magnetic dilution on the ferrimagnetic resonance of disordered heterostructures.* Journal of magnetism and magnetic materials, 2003. **264(1)**: p. 86-94.